


## Simple random matrix model for the vibrational spectrum of structural glasses

E. Stanifer, P. K. Morse, A. A. Middleton, and M. L. Manning\*  
*Department of Physics, Syracuse University, Syracuse, New York 13210, USA*

 (Received 27 April 2018; published 25 October 2018)

To better understand the surprising low-frequency vibrational modes in structural glasses, where the density of states  $D(\omega)$  deviates from mean field predictions, we study the spectra of a large ensemble of sparse random matrices where disorder is controlled by the distribution of bond weights and network coordination. We find  $D(\omega)$  has three regimes: a very low-frequency regime that can be predicted analytically using extremal statistics, an intermediate regime with quasilocalized modes, and a plateau in  $D(\omega)$ . When there is a finite probability of bond weights approaching zero strength, the intermediate regime displays a scaling consistent with  $D(\omega) \sim \omega^4$ , independent of network coordination and system size, just as in simulated structural glasses.

DOI: [10.1103/PhysRevE.98.042908](https://doi.org/10.1103/PhysRevE.98.042908)

### I. INTRODUCTION

The vibrational spectra of disordered glassy materials exhibit universal features. Although these features govern the mechanical response and provide insight into mechanisms for material failure, their origin remains poorly understood.

Perhaps the most well-studied feature of the density of vibrational states  $D(\omega)$  is the boson peak, which is an excess of vibrational modes above the Debye prediction,  $D(\omega) \propto \omega^{d-1}$  [1–3]. In jammed packings the frequency at which the peak occurs,  $\omega^*$ , scales linearly with the average excess number of contacts  $\delta z$  above the isostatic point where the number of constraints equals the degrees of freedom [2,4,5]. Additionally, the eigenvector statistics of modes in the boson peak follow a universal distribution [6].

Recently, another universal feature has been identified in simulations of low-dimensional jammed systems,  $D(\omega) \sim \omega^4$  below  $\omega^*$  [7–9], which deviates from recent mean-field calculations for the spectra in infinite dimensions that predict  $D(\omega) \sim \omega^2$  [10,11]. This interesting behavior has also been found in Heisenberg spin glass systems [12]. Understanding this regime is important, because the vibrational modes are quasilocalized and help govern flow and failure in disordered solids [1,12–17].

Given the success of random matrix theory in predicting universal features in other physical systems [18,19], it is natural to wonder if a random matrix model may also explain the  $\omega^4$  scaling in jammed packings. Other features, including the boson peak, have already been understood in terms of Euclidean random matrices, which are dynamical matrices for a set of points that are randomly and uniformly distributed in space [20].

Although there are generic arguments that the global minima of random functions should have a spectrum that scales as  $\omega^4$  [21], we would like to construct a random matrix model to provide insight into how features of the  $\omega^4$  region, such as the prefactor or the location of the scaling regime, change

with parameters such as the excess coordination  $\delta z$ . Such an understanding is important for predicting how material preparation protocols alter the mechanical response of glassy materials.

### II. RANDOM MATRICES

We study random matrices that share three important features with the dynamical matrix: they are symmetric, positive semidefinite, and force balancing. In higher dimensions, force balance corresponds to  $d$  sum rules on partial sums of entries in each row of a matrix, while in one dimension, the force-balancing restriction simply requires the sum over all the entries in a row must be zero [1]. This rule is also obeyed by standard or weighted Laplacians,  $L_{ij}$ , which are also symmetric and positive semidefinite. They are defined by

$$L_{ij} = \begin{cases} -k_{ij} & i \text{ and } j \text{ are connected,} \\ \sum_{l \neq i} k_{il} & i = j, \\ 0 & \text{otherwise,} \end{cases} \quad (1)$$

where  $k_{ij}$  is the independently chosen random weight of the edge between particles  $i$  and  $j$  and in the special case of the standard Laplacian,  $k_{ij} = 1$  [22]. Standard Laplacian matrices are well studied and possess distinctive vibrational spectra [23–26], so we focus on weighted Laplacians for the remainder of this article.

In order to calculate the Laplacian we must specify the topology of the underlying graph. Although recent advances have been made in analytically characterizing the spectra of Laplacians on an Erdős-Rényi graph [27,28], Erdős-Rényi networks are not locally isostatic, because a significant fraction of nodes are undercoordinated (fewer than isostatic coordination,  $z_c = 2d$ ), which leads to highly localized excitations that are not seen in jammed packings [27].

Instead, we consider the weighted Laplacian on a  $z_c$ -regular graph with a small number of additional edges, or crossbonds. Since weighted Laplacians obey only one sum rule, they are effectively one-dimensional (1D), and  $z_c = 2$ . The number of additional bonds is  $\delta z N$  where  $N$  is the number of points and  $\delta z$  is the excess coordination.

\*Corresponding author: [mlmanning@syr.edu](mailto:mlmanning@syr.edu)

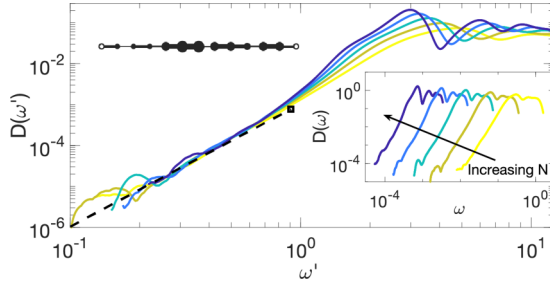


FIG. 1. The rescaled density of states,  $D(\omega')$  where  $\omega' = \omega N$ , for the two-regular graph with  $N = 16, 64, 256, 1024,$  and  $4096$  and  $\alpha = 0$ , normalized by system size,  $N$ , averaged over at least  $10^6$  matrices. The analytic prediction for the low-frequency scaling is shown as the black dashed line. In the upperleft we have a sketch of a 1D chain with periodic boundary conditions (the open circles are the same node) Inset: Unscaled density of states,  $D(\omega)$ .

Another important control parameter is the distribution of the edge weights and, in particular, the weight of this distribution near zero. We choose to parametrize this distribution as a power law with exponent  $\alpha$ , normalized so that the mean is 1,  $\rho(k) \propto k^\alpha$  on  $[0, \frac{\alpha+2}{\alpha+1}]$ . A uniform distribution corresponds to  $\alpha = 0$ , and we consider only normalizable distributions,  $\alpha > -1$ .

### A. Finite size scaling for the weighted ring

We first study the finite size scaling of the low-frequency excitations at isostaticity, when  $\delta z = 0$  and the underlying network topology is simply a ring of size  $N$ . Although this is a well-studied model, we believe its finite-size scaling can provide insight into the case with  $\delta z > 0$ .

The inset to Fig. 1 shows the sample averaged density of states for  $\alpha = 0$ , calculated via diagonalization of the matrix, as a function of system size  $N$ , averaged over  $2 \times 10^6$  matrices. The main panel shows the sample averaged density of states as a function of the normalized frequency,  $\omega' = \omega N$ , highlighting a region of power-law scaling at the lowest frequencies that disappears in the thermodynamic limit.

We hypothesize that the lowest-energy mode on a weighted ring is well approximated by a stretching of the two weakest bonds, with all other bond lengths relatively fixed. We expect this to be the case when  $\alpha \leq 0$ , so that the weight of the lowest two bonds are well separated from bonds with larger values of  $k_{ij}$ , especially in the limit of low  $\omega$ ,  $\omega < N^{-\frac{2\alpha+3}{4\alpha+3}}$ .

If the two weakest bonds have strengths  $k_1$  and  $k_2$  and are separated by  $m$  nodes, the frequency of this mode is  $\sqrt{\frac{N(k_1+k_2)}{m(N-m)}}$ . As we show in the appendices, one can use extremal statistics to find the exact distribution of the weakest bonds on the ring to predict that the low-frequency density of states scales as

$$D(\omega) \propto N^{2\alpha+3} \omega^{4\alpha+3}. \quad (2)$$

For a uniform distribution of bond weights ( $\alpha = 0$ ), the contribution of these modes to the density of states scales as  $(N\omega)^3$ . The scaling of Eq. (2), using  $\alpha = 0$ , is shown as the black dashed line in Fig. 1.

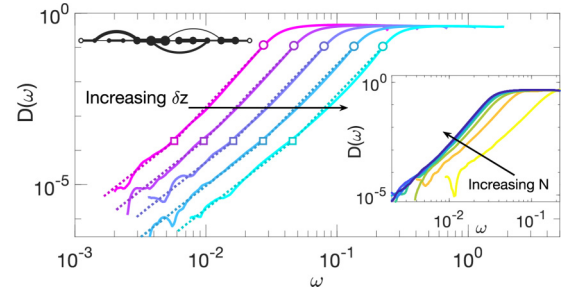


FIG. 2. The density of states for fixed system size ( $N = 1000$ ) and changing  $\delta z = 0.1, 0.168, 0.282, 0.476, 0.8$ . In the upper left we have a sketch of a 1D chain with periodic boundary conditions (the open circles are the same node) with additional bonds. Inset: The density of states,  $D(\omega)$ , for fixed  $\delta z = 0.1$  and changing system size  $N = 20, 60, 120, 240, 500, 1000, 2000,$  and  $4000$ .

### B. Crossbonded ring with uniform bond weights

We hypothesize that adding a small number of crossbonds alters the low-frequency behavior by reducing the effective distance between the two weakest bonds. In the case of  $\delta z = 0$ , the two weakest bonds separate the ring into two segments that can move relative to one another at nearly zero cost, but if a crossbond connects those two segments, it will significantly increase the energy of that mode. Therefore, the weak bonds that contribute to low-frequency modes must both be in a segment between crossbonds. Because there are  $N\delta z$  such segments, we expect that crossbonds give rise to an extensive number of low-energy modes, so that the scaling regime described in the previous section persists in the thermodynamic limit.

We search for very low-weight edges that generate a two-cut of the network: two edges that, if removed, disconnect the network. In the appendices, we show the low-frequency density of states scales as

$$D_\alpha(\omega) \propto \left(\frac{1}{\delta z}\right)^{2\alpha+3} \omega^{4\alpha+3}, \quad (3)$$

independent of system size. In this equation, the term  $\frac{1}{\delta z}$  takes the place of the term proportional to system size in the weighted ring [Eq. (2)]. The excess coordination effectively rescales the system, promoting a finite size effect seen in the vibrational spectrum of the ring to a thermodynamic property of the crossbonded system.

To test the universal form predicted by Eq. (3), we computed the spectrum  $D(\omega)$  for rings with crossbonds and uniform bond weights ( $\alpha = 0$ ). For each value of  $\delta z$  and  $N$  we generated between  $10^5$  and  $2 \times 10^6$  matrices, [29] with independently chosen weights and uniformly random placements of the endpoints of the  $N\delta z/2$  crossbonds. The inset to Fig. 2 displays plots of the sample-averaged density of states  $D(\omega)$  for fixed  $\delta z = 0.1$  as  $N$  increases. This example plot supports the convergence of  $D(\omega)$  to a gapless distribution as  $N \rightarrow \infty$ . The main panel of Fig. 2 displays the computed density of states (solid lines) for large  $N$  ( $N = 1000$ ) and varying  $\delta z$ . The dashed lines in Fig. 2 show fits of the form  $D(\omega) \propto \omega^3$  to the low-frequency region, as predicted by Eq. (3). These fits are in good agreement with the computed spectra.

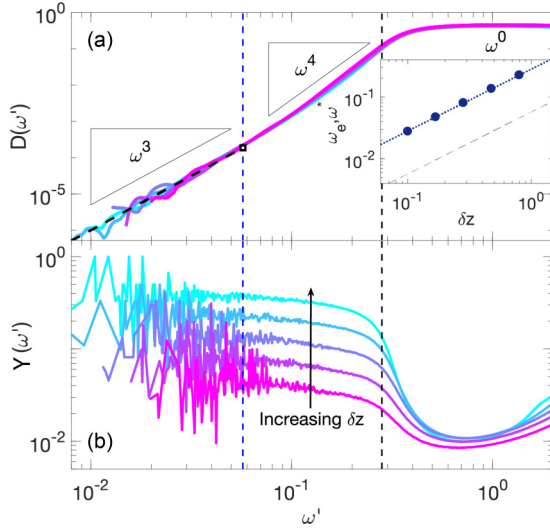


FIG. 3. (a) The density of states,  $D(\omega)$ , rescaled by  $\delta z$ ,  $\omega' = \omega/\delta z$ . The blue dashed line indicates the transition from the  $\omega^3$  regime to the  $\omega^4$  regime, and the black dashed line indicates the transition to the plateau. The inset shows the scaling of  $\omega^*$  and  $\omega_e$  with  $\delta z$  is linear. (b) The inverse participation ratio (IPR) rescaled by  $\delta z$ . The IPR approaches a quasilocalized plateau in the  $\omega^3$  region.

Based on Eq. (3) and the more complete form of the density of states derived in Appendix B, we expect a collapse of  $D(\omega)$  when frequencies are scaled by  $\delta z$ , for  $\alpha = 0$ . Figure 3(a) shows the density of states for the scaled frequency,  $\omega = \omega/\delta z$ . For  $\delta z = 0.168$  we numerically identify a frequency  $\omega_e$  that best separates the  $\omega^3$  scaling regime from the remaining spectrum. Equation (3) then predicts that all other cutoff frequencies should scale linearly with  $\delta z$ , which is in good agreement with the data as shown by the open squares in Figs. 2 and 3(a).

In addition to the crossover at  $\omega_e$ , there is a second crossover where  $D(\omega)$  flattens to a plateau. In jammed packings at zero temperature, where the boson peak occurs at the onset of the plateau,  $\omega^*$  is often defined as the frequency at which the density of states attains a fixed fraction  $f$  (typically 25%) of its value in the plateau [30]. We use that same definition here with  $f = 0.25$ .

In many disordered solids, numerical evidence suggests  $\omega^* \propto \delta z$  [2,5]. To check whether this is also true for our matrices, we plot the density of states as a function of the rescaled frequency  $\omega' = \omega/\delta z$ , for various values of  $\delta z$ , shown in Fig. 3(a). We see a good collapse of the three regions, suggesting that both crossovers are linear in  $\delta z$ , which is also highlighted by the inset to Fig. 3(a).

Importantly, this confirms that although the intermediate region between the two crossover frequencies spans less than a decade in frequency, it is well defined and does not change as a function of excess coordination or system size. Specifically, these results mandate the following functional form for the density of states in our random matrix model with  $\alpha = 0$ :

$$D(\omega) = \begin{cases} \left(\frac{\omega}{\delta z}\right)^3 & \omega \leq \omega_e \\ \propto \omega^\psi & \omega_e \leq \omega \leq \omega^* \\ \propto \text{const} & \omega^* \leq \omega \end{cases} \quad (4)$$

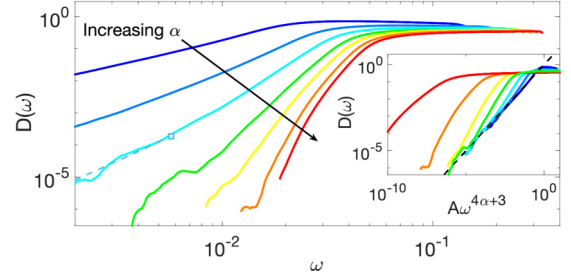


FIG. 4. The density of states for  $\alpha = -0.4, -0.2, 0, 0.25, 0.5, 1$ , and  $2$ , with  $\delta z = 0.1$ . Inset:  $D(\omega' = A\omega^{4\alpha+3})$  for the same values of  $\alpha$  as in the main figure, where  $A$  is the coefficient predicted in Appendix B. The black dashed line is the predicted scaling for the low-frequency regime.

To extract the scaling of  $D(\omega)$  below the boson peak, we fit  $D(\omega)$  to this functional form and extract the best-fit  $\psi$  for each value of  $\delta z$  (see Table I in Appendix B). We find that all curves are consistent with  $\psi = 4.0 \pm 0.05$  for frequencies  $\omega_e \leq \omega \leq \omega^*$ . This suggests  $D(\omega) \propto \omega^4$ , just as seen below the plateau in simulations of jammed packings.

Given the striking similarities between the density of states in this simple model and jammed packings, we would also like to know if the eigenvector statistics are similar. In jammed systems, many modes at frequencies below the boson peak are quasilocalized [30]. This is quantified by the inverse participation ratio (IPR),  $Y(\omega) = \sum_i v_i^4 / (\sum_i v_i^2)^2$ , where  $v$  is the vector associated with the eigenfrequency  $\omega$ . In Fig. 3(b) the very low-frequency regime of the IPR plateaus, and the value of this plateau scales with  $\delta z$ , indicating that only about  $\frac{1}{\delta z}$  nodes are participating in the vibration. We have also shown in the appendices that the value of the IPR is independent of system size in this quasilocalized regime.

Interestingly, the intermediate region exhibits values of IPR that are typically associated with quasilocalized excitations. Moreover, the size of those excitations seems to decrease as  $\delta z$  increases. In jammed solids, an outstanding open question is how the size of localized excitations changes as one approaches the jamming transition.

### C. Crossbonded ring with power-law bond weights

Having a simple constructive model that reproduces many features of the vibrational modes in jammed packings is useful, because we can vary the model and ask what features are necessary to generate the  $\omega^4$  scaling in the density of states. One natural choice is to perturb the distribution of bond strengths away from the uniform distribution by changing the power-law exponent  $\alpha$ .

For  $\alpha > 0$ , very weak bonds become rare, and the assumptions that lead to Eq. (3) break down. Numerically, we observe that a gap appears to open up in the spectrum as  $\alpha$  increases, as seen in Fig. 4. For  $\alpha < 0$ , we expect Eq. (3) should still hold, as shown by the numerical data in the inset of Fig. 4. In this case, however, the crossover frequency no longer scales linearly with  $\delta z$ , and so the power-law scaling between  $\omega_e$  and  $\omega^*$ , the exponent  $\psi$  in Eq. (4), is no longer independent of  $\delta z$ . In other words, an intermediate regime consistent with  $D(\omega) \propto \omega^4$ , independent of  $\delta z$ , is possible



only for  $\alpha = 0$ . It seems that having finite probability of bonds with weight approaching zero provides for approximate  $\omega^4$  scaling.

### III. DISCUSSION

In this article, we propose a simple random matrix model that is locally nearly isostatic and captures features of the vibrational states of disordered packings that are typically associated with marginality. Specifically, the model recapitulates a plateau in the density of states above  $\omega^*$  and a regime consistent with  $\omega^4$  scaling immediately below that. Our model also has a second crossover frequency  $\omega_e$ , below which  $D(\omega)$  scales as  $\omega^3$ .

The modes in this extremely low-frequency regime are governed by extremal statistics, and so we can calculate their properties analytically. This allows us to demonstrate that  $\omega_e$  scales linearly with excess coordination  $\delta z$  if and only if the weak bonds are uniformly distributed, suggesting that  $\omega^4$  seen in jammed packings arises due to a special, self-organized distribution of the weakest bonds.

Of course, jammed packings only exist in dimensions greater than unity. Above one dimension, the bond between particles is described by a tensor and not a scalar weight. The  $d$  by  $d$  interaction block that corresponds to a single bond in the Hessian matrix can be written as  $H_{ij\alpha\beta} = -V''|u_{\parallel}|^2 - \frac{V'}{r_{ij}}|u_{\perp}|^2$ . The first term is often referred to as the stiffness, while the second term is called the prestress term [31].

Interestingly, observations in three-dimensional jammed packings suggest that the  $\omega^4$  regime exists only when the  $V'$  term is unperturbed; even very small perturbations to the prestress [3] open up a gap in the density of states [32]. This suggests that a self-organized balance between the stiffness and prestress must occur in systems near isostaticity. Moreover, the stiffness is always positive, and the prestress always decreases the entries in the Hessian, so it is plausible that the prestress term is driving some interactions to be very weak near isostaticity. This is similar to our simple model where self-organized weak interactions also dominate the low-energy excitations. Therefore, it may be the case that the fine-tuning of  $\alpha$  necessary in our model corresponds to fine-tuning in the prestress in real glasses. To investigate this possibility, future research will focus on studying the statistics of interparticle interactions to quantify the effective stiffness of bonds [33] in simulated glasses as the prestress is perturbed away from marginality [3].

In addition, a more concrete connection will require us to extend the insight from our simple model to higher dimensions. We see an  $\omega^4$  regime when bond strengths are uniform, but it is unclear what quantity would be analogous to a uniform bond weight in a  $d \times d$  subblock in a random matrix. Concurrent work by Benetti *et al.* focused on  $d$ -dimensional Laplacian matrices where the magnitude of each bond is unity, but the geometry of the bond is randomly distributed, and these also generate scaling consistent with  $\omega^4$  at low frequencies [34]. Benetti *et al.* show this scaling in a higher-dimensional model also requires a network that is

nearly isostatic. We are hopeful that in future work we may be able to connect our analytic results to these numerical ones in higher dimensions. One possible avenue is to study whether the geometric disorder in the model by Benetti *et al.* requires some interactions between nodes to be effectively zero along special soft directions.

Furthermore, although  $\omega^4$  scaling as been observed in several glass-forming systems [7], the  $\omega^3$  regime may be unique to 1D systems, because it has not been reported in simulations or in the random matrices with  $3 \times 3$  subblocks [34]. In addition, we see about half a decade of frequency consistent with  $\omega^4$  scaling, while the most recent data from Lerner and collaborators [7,9,32] find almost a full decade.

Nevertheless, the  $\omega^3$  scaling regime is interesting. Disordered rings are well studied, but major results focus on localization caused by disorder [35,36]. To our knowledge, the finite-size scaling effects of the vibrational spectrum have not been discussed previously. Our model demonstrates that finite-size effects in the disordered ring, such as this gapless low-frequency scaling, can be promoted into properties that are maintained in the thermodynamic limit by network disorder.

Although we have excellent understanding of the  $\omega^3$  regime in this simple model, and convincing numerical evidence demonstrating  $D(\omega)$  is consistent with  $\omega^4$  scaling over a window of about half of a decade in  $\omega$ , we have not identified a mechanism to understand this regime, where we know the assumption of two weak bonds and two rigid arms breaks down. In this analysis we have restricted ourselves to two-cuts, where only two weak bonds are involved in a mode. However, one can consider higher order cuts, where we remove more than two bonds and yet which still have relatively low energies. These higher order cuts have been left for future work due to the specialized techniques for finding such partitions, like spectral clustering [37], which are beyond the scope of this work.

One possible avenue for understanding this regime is suggested by recent numerical work that shows universality in the eigenvector statistics associated with the boson peak. Specifically, eigenstatistics in jammed packings match those from both the random matrix model described here, as well as the dense limit of this model where all nodes are connected to one another [6]. Interestingly, the eigenvector statistics are also identical in a much simpler model which is just the sum of a diagonal matrix and a Gaussian orthogonal matrix. Very recent analytic work suggests that such matrices are marginal; they are on the edge of a nonergodic localized phase [38]. It would therefore be very interesting to extend this analytic work to sparse matrices and study the tail of the density of states.

Another way to extend our model is to alter the loop structure of the underlying graph. In our random matrix model, the loop structure is uncontrolled since we add crossbonds with uniform probability across the graph. This is different from jammed systems where neighbors of one particle are more likely to be neighbors of each other and loops are small. It is fairly straightforward to extend our analytic analysis of the  $\omega^3$  regime to random matrix models with smaller loops, and we expect that the prefactor and the onset of the scaling  $\omega_e$

will change, but the  $\omega^3$  scaling will not. However, this change could impact the behavior of the  $\omega^4$  regime.

### ACKNOWLEDGMENTS

We thank Fernanda Benetti, Gabriele Sicuro, and Giorgio Parisi for discussions. This work was partially supported by the Simons Foundation Grant No. 454947 (E.S., P.M., M.L.M.) and by NSF-DMR-1352184 (E.S., M.L.M.). Computational resources were provided by support from Syracuse University and NSF ACI-1541396.

### APPENDIX A: EXTREMAL STATISTICS IN THE TWO-REGULAR GRAPH

In this appendix, we calculate the scaling for a ring of  $N$  particles and a ring with crossbonds where particles are bonded to their nearest neighbors and the strengths of those bonds,  $\{b_i\}$ , are chosen independently with the distribution  $f(b)$ . (It is also assumed that the masses of the particles are identical.)

The mode associated with exciting only the two weakest bonds is a very low-energy mode. The calculation here is done by taking the two weakest bonds as they are, but assuming all other bonds are rigid. A simple sketch highlighting the weakest bonds is shown in Fig. 5.

We will call the strength of these bonds  $k_1$  and  $k_2$  with a distance of  $m$  nodes between the bonds. This system is equivalent to two masses joined by a spring which has one nontrivial mode with a frequency of  $\sqrt{\frac{N(k_1+k_2)}{m(N-m)}} \equiv \sqrt{\frac{Ns}{m(N-m)}}$  where  $s = k_1 + k_2$ .

The distribution of the weakest bond strength is given by

$$\rho_1(k_1) = Nf(k_1)[1 - F(k_1)]^{N-1}, \quad (\text{A1})$$

which is just the probability density of a bond having strength  $k_1$  multiplied by the probability that all other bonds are at least that strong [39]. The distribution of the second lowest mode is somewhat more complicated since we need to enforce that  $k_2 \geq k_1$ . So the distribution of  $k_2$  given  $k_1$  is

$$\rho_2(k_2|k_1) = \frac{(N-1)\theta(k_2 - k_1)}{[1 - F(k_1)]^{N-1}} f(k_2)[1 - F(k_2)]^{N-2}. \quad (\text{A2})$$

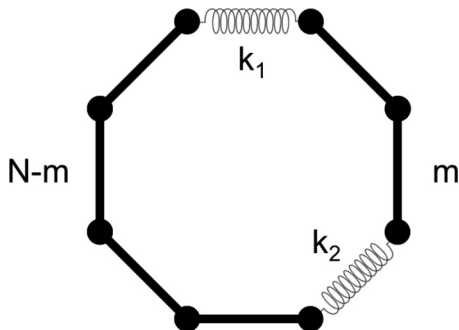


FIG. 5. A ring or periodic 1D spring system with the two weakest bonds highlighted as springs.

The frequency depends on the sum  $s = k_1 + k_2$ . The distribution of this sum can be obtained from the convolution of the distribution of  $k_1$  and  $k_2$ :

$$\rho_s(s) = \int_{k_{\min}}^{k_{\max}} \rho_1(k_1)\rho_2(s - k_1, k_1) dk_1, \quad (\text{A3})$$

$$\rho_s(s) = N(N-1) \int_{k_{\min}}^{k_{\max}} f(k_1)f(s - k_1) \times [1 - F(s - k_1)]^{N-2} \theta(s - 2k_1) dk_1. \quad (\text{A4})$$

By changing variables and assuming  $m$  is uniformly distributed, we can obtain the distribution of the frequencies as

$$\rho_\omega(\omega) = \sum_{m=1}^{N-1} \rho_s\left(\frac{m(N-m)}{N}\omega^2\right) \frac{2m(N-m)}{N(N-1)}\omega. \quad (\text{A5})$$

#### 1. Power-law distribution

Let  $f(b) = \frac{\alpha+1}{L^{\alpha+1}}b^\alpha$  and  $F(b) = \left(\frac{b}{L}\right)^{\alpha+1}$  under the limit  $b \in [0, L]$  and  $\alpha > -1$ . In the main text, we define  $L = \frac{2+\alpha}{1+\alpha}$  such that the mean of the distribution is 1. By substitution, we find

$$\rho_s(s) = \frac{N(N-1)(\alpha+1)^2}{L^{2(\alpha+1)}} \int_0^L \theta(s - k_1)\theta(L - s + k_1) \times \theta(s - 2k_1)k_1^\alpha (s - k_1)^\alpha \left[1 - \left(\frac{s - k_1}{L}\right)^{\alpha+1}\right]^{N-2} dk_1. \quad (\text{A6})$$

These step functions are only nonzero in the range  $\max(0, s - L) \leq k_1 \leq s/2$ . Using this information and a change of variables,  $k = sq$ , we can extract the primary contribution of  $s$ :

$$\rho_s(s) = s^{2\alpha+1} \frac{N(N-1)(\alpha+1)^2}{L^{2(\alpha+1)}} \theta\left(L - \frac{s}{2}\right) \times \int_{\max(0, 1 - \frac{s}{L})}^{\frac{1}{2}} q^\alpha (1 - q)^\alpha \left\{1 - \left[\frac{s(1 - q)}{L}\right]^{\alpha+1}\right\}^{N-2} dq. \quad (\text{A7})$$

Under the assumption that  $s$  is small, such that  $\left\{1 - \left[\frac{s(1 - q)}{L}\right]^{\alpha+1}\right\}^{N-2} \approx 1$  (we will discuss the range of validity of this assumption below), the density of states for large  $N$  can be found via direct integration of  $\int_0^{\frac{1}{2}} [q(1 - q)]^\alpha dq = \frac{\Gamma(\alpha+1)^2}{2\Gamma(2\alpha+2)}$ .

$$\rho_s(s) \approx s^{2\alpha+1} \frac{N(N-1)(\alpha+1)^2}{L^{2(\alpha+1)}} \frac{\Gamma(\alpha+1)^2}{2\Gamma(2\alpha+2)}, \quad (\text{A8})$$

$$\rho_\omega(\omega) \approx \frac{N\Gamma(\alpha+1)^2(\alpha+1)^2}{\Gamma(2\alpha+2)L^{2\alpha+2}} \omega^{4\alpha+3} \sum_{m=1}^{N-1} \left[\frac{m(N-m)}{N}\right]^{2\alpha+2}. \quad (\text{A9})$$

By converting the sum over  $m$  into a similar integral over  $\frac{m}{N}$  we have

$$\rho_\omega(\omega) \approx \frac{\sqrt{\pi}(\alpha+1)^2(2\alpha+2)\Gamma(\alpha+1)^2}{2^{4\alpha+5}\Gamma(2\alpha+\frac{7}{2})L^{2\alpha+2}} N^{2\alpha+4} \omega^{4\alpha+3}. \quad (\text{A10})$$

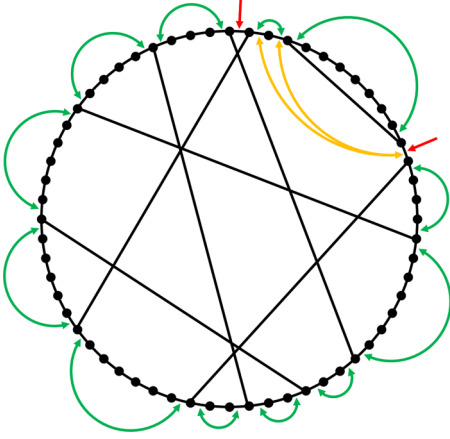


FIG. 6. A sketch of a crossbonded network with 56 particles and seven crossbonds. The green arrows delineate the regions between crossbonds where two edges can disconnect the network. The red arrows point out edges that can't disconnect the network. The yellow arrows point out sets of edges that would disconnect the network that aren't between crossbonded nodes.

Since this applies only to the lowest vibrational mode, the density of states is given by  $\rho_\omega/N$ :

$$D(\omega) \approx \frac{\sqrt{\pi}(\alpha+1)^2(2\alpha+2)\Gamma(\alpha+1)^2}{2^{4\alpha+5}\Gamma(2\alpha+\frac{7}{2})L^{2\alpha+2}} N^{2\alpha+3} \omega^{4\alpha+3}. \quad (\text{A11})$$

## APPENDIX B: EXTREMAL STATISTICS IN THE TWO-REGULAR GRAPH WITH ADDITIONAL BONDS

A more generic system is the ring with crossbonds. These crossbonds are simply additional connections between particles that are nonadjacent in the ring. See Fig. 6 for an example of a nonbonded graph; although the sketch is two-dimensional, the crossbond interaction depends only on the distance along the ring, not the Euclidean distance across the ring.

With crossbonds, we are restricted to choosing bonds in a region between two crossbonded nodes. These regions are shown in Fig. 6 by the green arrows.

### 1. Distribution of bounded regions

Let  $m_1$  be the number of edges between crossbonded nodes.

We place the crossbonds randomly. Therefore the crossbonded nodes are chosen uniformly. If we have  $E$  crossbonds, then there are  $2E$  crossbonded nodes (which may not be unique). The increase in average coordination number is given by  $\delta z = \frac{2E}{N}$ . So the number of crossbonds and crossbonded nodes are  $\frac{N\delta z}{2}$  and  $N\delta z$ , respectively.

Since these are uniformly placed, we can expect the distance between them to be defined via a Poisson process. We can find the distribution of the second crossbonded node where we set the first crossbonded node to 1, since we can always rotate along the ring. Order statistics provide the

following result:

$$p_1(m_1) = \frac{\left(1 - \frac{m_1}{N}\right)^{N\delta z - 1}}{\sum_{m=0}^{N-1} \left(1 - \frac{m}{N}\right)^{N\delta z - 1}} \approx \frac{e^{\delta z} - 1}{e^{\delta z}} e^{-m_1 \delta z}. \quad (\text{B1})$$

This distribution very quickly approaches the thermodynamic expression of an exponential decay.

### 2. Crossbonded spectrum

For each chain of length  $m_1$ , we choose the two weakest bonds where the bonds are chosen from the distribution  $f(b) = \frac{\alpha+1}{L^{\alpha+1}} b^\alpha$  under the limit  $b \in [0, L]$  and  $\alpha > -1$ . In the main text, we define  $L = \frac{2+\alpha}{1+\alpha}$  such that the mean of the distribution is 1. We can write  $\rho_s(s)$  as

$$\rho_s^{m_1}(s) = \frac{(\alpha+1)^2 m_1 (m_1 - 1)}{L^{2(\alpha+1)}} s^{2\alpha+1} \theta\left(L - \frac{s}{2}\right) \times \int_{\max(0, 1-\frac{s}{L})}^{\frac{1}{2}} q^\alpha (1-q)^\alpha \left\{1 - \left[\frac{s(1-q)}{L}\right]^{\alpha+1}\right\}^{m_1-2} dq. \quad (\text{B2})$$

We assume small  $s$ , such that  $\left\{1 - \left[\frac{s(1-q)}{L}\right]^{\alpha+1}\right\}^{m_1-2} \approx 1$ . Following the same argument from the previous section where  $m_2$  is the number of nodes between the weakest bonds, we find the distribution:

$$\rho_\omega(\omega) = \omega^{4\alpha+3} \frac{\Gamma(\alpha+1)^2 (\alpha+1)^2 e^{\delta z} - 1}{2\Gamma(2\alpha+2)L^{2\alpha+2}} \frac{1}{e^{\delta z}} \times \sum_{m_1=2}^{N-1} e^{-m_1 \delta z} m_1 \sum_{m_2=1}^{m_1-1} \left[\frac{m_2(N-m_2)}{N}\right]^{2\alpha+2}. \quad (\text{B3})$$

We take the thermodynamic limit and approximate the sums as integrals (over  $x = \frac{m_i}{N}$  and  $dx = \frac{1}{N}$ ) and expand the result in the low  $\delta z$  limit to obtain

$$\rho_\omega(\omega) = \frac{\Gamma(2\alpha+5)\Gamma(\alpha+1)^2(\alpha+1)^2 \omega^{4\alpha+3}}{2(2\alpha+3)\Gamma(2\alpha+2)L^{2\alpha+2} \delta z^{2\alpha+4}}. \quad (\text{B4})$$

Importantly, this is not just for the smallest mode. Since there are several regions on the ring from which pairs can be chosen, this analysis an extensive fraction of modes. On average, there are  $N\delta z$  regions separated by crossbonded nodes. Therefore, we can apply this analysis for the lowest  $N\delta z$  modes of a total  $N$  modes, i.e., a fraction of modes  $\delta z$ . The density of states is given by  $\rho_\omega(\omega) * \delta z$ :

$$D_\alpha(\omega) = \frac{\Gamma(2\alpha+5)\Gamma(\alpha+1)^2(\alpha+1)^2 \omega^{4\alpha+3}}{2(2\alpha+3)\Gamma(2\alpha+2)L^{2\alpha+2} \delta z^{2\alpha+3}}. \quad (\text{B5})$$

TABLE I. Best fit to our numerical data for the scaling exponent  $\psi$  in Eq. (B7), for different values of  $\delta z$ .

$\delta z$	$\psi$
0.1	4.0761
0.168	4.0115
0.282	3.9606
0.476	3.9496
0.8	3.9749

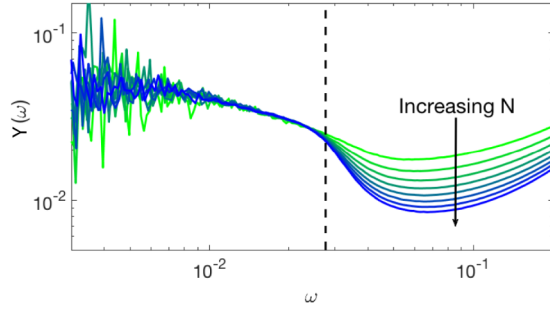


FIG. 7. IPR at a fixed  $\delta z = 0.1$ , with system sizes varying from 300 to 1000 in steps of 100. The black dashed line indicates  $\omega^*$ .

Note that  $\alpha = 0$ , the uniform distribution, is unique in that  $\omega$  and  $\delta z$  have the same exponent

$$D_0(\omega) = \frac{4}{L^2} \left( \frac{\omega}{\delta z} \right)^3. \quad (\text{B6})$$

### 3. Full spectrum

In the full spectrum we need to identify the frequency,  $\omega^*$ , at which the spectrum crosses over into a plateau. In disordered solids, there are ample examples of this cutoff scaling linearly with  $\delta z$ ; this is also true for the disordered ring with crossbonds.  $\omega_e$  scales linearly with  $\delta z$  for only  $\alpha = 0$ . Therefore it is only for  $\alpha = 0$  that the scaling between  $\omega_e$  and  $\omega^*$ ,  $\psi$ , is independent of  $\delta z$ .

So the full spectrum of  $\alpha = 0$  is given by

$$D(\omega) = \begin{cases} \frac{4}{L^2} \left( \frac{\omega}{\delta z} \right)^3 & \omega \leq \omega_e \\ \left( \frac{4\omega_e^{3-\psi}}{L^2 \delta z^3} \right) \omega^\psi & \omega_e \leq \omega \leq \omega^* \\ c & \omega^* \leq \omega \end{cases}. \quad (\text{B7})$$

In practice,  $\psi$  is consistent with 4, see Table I. After finding the  $\omega_e/\delta z$  that best separates the low frequency regime for  $\delta z = 0.168$ , chosen for numerical stability, and using this ratio for all  $\delta z$  values, we find the scaling in the intermediate regime is consistent with 4 independent of  $\delta z$ .

### 4. Behavior of sloshing modes

The value of the IPR for a sloshing modes depends explicitly on the distance between the active bonds. If the active

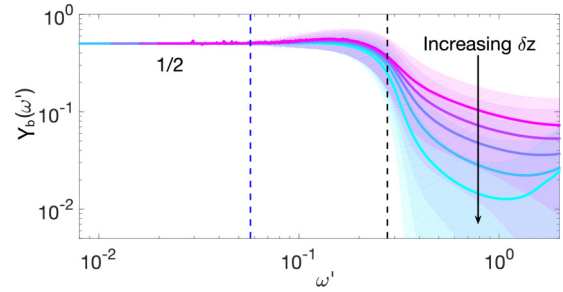


FIG. 8. The BIPR with the frequency rescaled by  $\delta z$ ,  $\omega' = \omega/\delta z$ . The blue dashed line indicates  $\omega_e$ , and the black dashed line indicates  $\omega^*$ .

bonds are separated by  $m$  particles, the IPR is given by

$$Y = \frac{1}{m} + \frac{1}{N-m} - \frac{3}{N}. \quad (\text{B8})$$

Thus the increasing of the IPR plateau with  $\delta z$  in the sloshing regime is indicative of a decrease in the distance between active bonds. By construction of the crossbonded system, the distance between active bonds is limited by the distance between crossbonded nodes, which decreases with  $\delta z$ .

Figure 7 shows the IPR for varying system sizes, indicating that the IPR is independent of system size in the low-frequency regime, while modes in the boson peak are strongly dependent on system size. We find that the low-frequency regime collapses, and the behavior of the system below  $\omega^*$  is independent of system size.

We can also measure the participation of the bonds with what we call the bond inverse participation ratio (BIPR):

$$Y_b(\omega) = \frac{\sum_{(i,j)} (v_i - v_j)^4}{\left( \sum_{(i,j)} (v_i - v_j)^2 \right)^2}, \quad (\text{B9})$$

where  $(i, j)$  is an edge in the network. In the limit of low frequency, there is a plateau of  $\text{BIPR} = \frac{1}{2}$ , as seen in Fig. 8, which indicates that only two bonds are extending or compressing for the modes in that regime. This is secondary confirmation that the sloshing mode assumption is reasonable for this simple model.

[1] M. L. Manning and A. J. Liu, *Phys. Rev. Lett.* **107**, 108302 (2011).  
 [2] C. S. O'Hern, L. E. Silbert, A. J. Liu, and S. R. Nagel, *Phys. Rev. E* **68**, 011306 (2003).  
 [3] E. DeGiuli, A. Laversanne-Finot, G. Düring, E. Lerner, and M. Wyart, *Soft Matter* **10**, 5628 (2014).  
 [4] M. Wyart, S. R. Nagel, and T. A. Witten, *Europhys. Lett.* **72**, 486 (2005).  
 [5] L. E. Silbert, A. J. Liu, and S. R. Nagel, *Phys. Rev. Lett.* **95**, 098301 (2005).  
 [6] M. L. Manning and A. J. Liu, *Europhys. Lett.* **109**, 36002 (2015).

[7] E. Lerner, G. Düring, and E. Bouchbinder, *Phys. Rev. Lett.* **117**, 035501 (2016).  
 [8] H. Mizuno, H. Shiba, and A. Ikeda, *Proc. Natl. Acad. Sci. USA* **114**, E9767 (2017).  
 [9] G. Kapteijns, E. Bouchbinder, and E. Lerner, *Phys. Rev. Lett.* **121**, 055501 (2018).  
 [10] P. Charbonneau, E. I. Corwin, G. Parisi, A. Poncet, and F. Zamponi, *Phys. Rev. Lett.* **117**, 045503 (2016).  
 [11] G. Parisi and F. Zamponi, *Rev. Mod. Phys.* **82**, 789 (2010).  
 [12] M. Baity-Jesi, V. Martín-Mayor, G. Parisi, and S. Perez-Gaviro, *Phys. Rev. Lett.* **115**, 267205 (2015).  
 [13] S. Wijtmans and M. L. Manning, *Soft Matter* **13**, 5649 (2017).

- [14] A. Tanguy, B. Mantsi, and M. Tsamados, *Europhys. Lett.* **90**, 16004 (2010).
- [15] M. Tsamados, A. Tanguy, F. Léonforte, and J. L. Barrat, *Eur. Phys. J. E* **26**, 283 (2008).
- [16] D. J. Ashton and J. P. Garrahan, *Eur. Phys. J. E* **30**, 303 (2009).
- [17] C. Brito and M. Wyart, *J. Stat. Mech.* (2007) L08003.
- [18] H. S. Camarda and P. D. Georgopoulos, *Phys. Rev. Lett.* **50**, 492 (1983).
- [19] M. Mehta, *Random Matrices*, Pure and Applied Mathematics (Elsevier Science, Amsterdam, 2004).
- [20] G. Parisi, *Eur. Phys. J. E* **9**, 213 (2002).
- [21] V. Gurarie and J. T. Chalker, *Phys. Rev. B* **68**, 134207 (2003).
- [22] R. Merris, *Linear Algebra Appl.* **197-198**, 143 (1994).
- [23] T. Aspelmeier and A. Zippelius, *J. Stat. Phys.* **144**, 759 (2011).
- [24] L. Erdős, A. Knowles, H.-T. Yau, and J. Yin, *Ann. Probab.* **41**, 2279 (2013).
- [25] L. Erdős, A. Knowles, H.-T. Yau, and J. Yin, *Commun. Math. Phys.* **314**, 587 (2012).
- [26] B. Mohar, *Theor., Combinat., Applic.* **2**, 871 (1991).
- [27] P. Erdős and A. Rényi, *Publ. Math. Debrecen* **6**, 290 (1959).
- [28] G. M. Cicuta, J. Krausser, R. Milkus, and A. Zaccone, *Phys. Rev. E* **97**, 032113 (2018).
- [29] For  $\delta z = 0.1$  and  $N = 500$  and  $1000$ , we calculate  $2 \times 10^6$  matrices, and for  $N = 2000$  and  $4000$ , we calculate 522 240 and 261 120 matrices. For all other values, we calculate  $10^6$  matrices.
- [30] N. Xu, V. Vitelli, A. J. Liu, and S. R. Nagel, *Europhys. Lett.* **90**, 56001 (2010).
- [31] W. G. Ellenbroek, Response of Granular Media near the Jamming Transition, Leiden Institute of Physics, Institute-Lorentz for Theoretical Physics, Faculty of Science, Leiden University (2007).
- [32] E. Lerner and E. Bouchbinder, *Phys. Rev. E* **97**, 032140 (2018).
- [33] E. Lerner and E. Bouchbinder, *J. Chem. Phys.* **148**, 214502 (2018).
- [34] F. P. C. Benetti, G. Parisi, F. Pietracaprina, and G. Sicuro, *Phys. Rev. E* **97**, 062157 (2018).
- [35] F. J. Dyson, *Phys. Rev.* **92**, 1331 (1953).
- [36] P. Dean, *Proc. Phys. Soc.* **84**, 727 (1964).
- [37] U. von Luxburg, *Stat. Comput.* **17**, 395 (2007).
- [38] D. Facoetti, P. Vivo, and G. Biroli, *Europhys. Lett.* **115**, 47003 (2016).
- [39] J. E. Gentle, *Computational Statistics (Statistics and Computing)* (Springer, New York, 2009).